# Crystal Structure of the Di-iron/Radical Protein of Ribonucleotide Reductase from *Corynebacterium ammoniagenes*[†,‡]

Martin Högbom,[§] Yasmin Huque,[||] Britt-Marie Sjöberg,[||] and Pär Nordlund*[,§]

*Department of Biochemistry and Biophysics, Arrhenius Laboratories A4, and Department of Molecular Biology and Functional Genomics, Arrhenius Laboratories F3, Stockholm University, SE-10691 Stockholm, Sweden*

*Received July 9, 2001; Revised Manuscript Received November 16, 2001*

ABSTRACT: Ribonucleotide reductase (RNR) is the enzyme performing de novo production of the four deoxyribonucleotides needed for DNA synthesis. All mammals as well as some prokaryotes express the class I enzyme which is an $\alpha_2\beta_2$ protein. The smaller of the homodimers, denoted R2, contains a di-iron carboxylate site which, upon reaction with molecular oxygen, generates a stable tyrosyl radical needed for catalysis. The three-dimensional structure of the oxidized class Ib RNR R2 from *Corynebacterium ammoniagenes* has been determined at 1.85 Å resolution and refined to an *R*-value of 15.8% ($R_{free}$ = 21.3%). In addition, structures of both the reduced iron-containing, and manganese-substituted protein have been solved. The *C. ammoniagenes* R2 has been proposed to be manganese-dependent. The present structure provides evidence that manganese is not oxidized by the protein, in agreement with recent biochemical data, and that no obvious structural abnormalities are seen in the oxidized and reduced iron-containing forms, giving further support that the protein is indeed an iron-dependent RNR R2. The di-manganese structure also provides an explanation for the magnetic properties of this site. The structure of the oxidized *C. ammoniagenes* R2 also reveals an additional water molecule bridging the radical and the iron site, which has not previously been seen in any other R2 structure and which might have important mechanistic implications.

The replication of all living cells requires deoxyribonucleotides for DNA synthesis. These building blocks are provided de novo by reduction of the corresponding ribonucleotides, a reaction catalyzed by the enzyme ribonucleotide reductase (*1*). The ribonucleotide reductases known today are divided into three classes (I−III). Class I is further divided into two subclasses, classes Ia and Ib, which both consist of two homodimeric proteins. The larger of the proteins carries the substrate binding site and the allosteric site. It is coded by *nrdA* in class Ia and by *nrdE* in class Ib. The proteins of the different subclasses are called R1 and R1E, respectively. In class Ia, the small subunit is coded by the gene *nrdB* and is called R2. In class Ib, it is coded by *nrdF* and called R2F.[1] This protein carries a dinuclear iron site and a stable tyrosyl radical essential for reduction of ribonucleotides.

R2(F) is one of several redox-active di-iron carboxylate proteins; the first ligand sphere around the metal center is conserved among these proteins (*2*). The di-iron carboxylate proteins perform excessively difficult oxygen-dependent chemistry, such as the desaturation of fatty acids and the hydroxylation of methane to methanol, involving highly reactive intermediates (*2*). The role of the iron site in R2 is to form the active cofactor, consisting of an oxidized metal site and the tyrosyl radical.

The formation of the active iron site in protein R2 can be studied in vitro in the $Fe^{2+}/O_2$ reconstitution reaction of apoR2. The suggested reaction mechanism is based on spectroscopic and structural investigations of the R2 from *Escherichia coli* (amino acid numbering below) and mouse. Two ferrous irons bind to the metal site forming the reduced [Fe(II)Fe(II)] state of the protein; this structure has previously been solved by X-ray crystallography (*3*). The reduced center proceeds through several redox states after being activated by molecular oxygen. Oxygen is suggested to bind to the ions in a bridging fashion and oxidize the two ions, forming a peroxo−ferric complex [Fe(III)−O−O−Fe(III)], which has been characterized in the R2 mutant (W48F/D84E) by vibrational spectroscopy (*4*) and in D84E by UV−vis and Mössbauer spectroscopy (*5*). After cleavage of the peroxo bridge and rearrangement of the oxygen atoms, one oxygen forms a $\mu$-oxo bridge between the irons, and one is terminally bound to one of the irons (*6*−*8*). In the di-iron carboxylate protein methane monooxygenase (MMO), a diamond core structure with the redox state Fe(IV)Fe(IV), named species Q, is formed after cleavage of the peroxo bridge (*9*). This intermediate has not been observed in R2, presumably because the oxygen bond cleavage occurs coupled to a rapid electron transfer from the protein surface to the metal site,

[†] This work was supported by grants from the Swedish Research Council for Technical Sciences (TFR), the Swedish Research Council for Natural Sciences (NFR), and the European Union EU-TMR (Contract FMRX-CT98-0207).

[‡] The atomic coordinates described in this paper have been deposited in the Protein Data Bank, entries 1KGN (oxidized Fe containing form), 1KGO (reduced Fe containing form), and 1KGP (Mn substituted form).

* Corresponding author. E-mail: Par.Nordlund@dbb.su.se. Telephone: +46-8-164141. Fax: +46-8-153679.

[§] Arrhenius Laboratories A4.

[||] Arrhenius Laboratories F3.

[1] Abbreviations: IMP, inositol monophosphate; MMO, methane monooxygenase; PRPP, 5-phospho-α-D-ribosyl-1-pyrophosphate; RNR, ribonucleotide reductase; R2(F), ribonucleotide reductase R2 and R2F proteins; SHE, standard hydrogen electrode.

10.1021/bi011429l CCC: $22.00 
Published on Web 12/29/2001

leading to a reduction. The redox state of the intermediate trapped in R2, named species X, is formally Fe(IV)−O−Fe(III)−O(H) (*8*). This species oxidizes a neighboring tyrosine residue, which forms the radical essential for ribonucleotide reduction. This is the active form of the metal cofactor, which carries the ferric [Fe(III)Fe(III)] state together with the Y122 radical (*10*). The tyrosyl radical is more easily reduced than the iron cluster; $E = 1000 \pm 100$ mV vs standard hydrogen electrode (SHE) compared to $E_m = -115 \pm 2$ mV vs SHE, respectively (*11*). Accordingly, a form of R2 in which the tyrosine is reduced, but the iron site is oxidized (MetR2), exists. The available oxidized structures of R2 are in the met form. Recently a detailed mechanism at the structural level for the oxygen activation and radical generation at these di-iron carboxylate sites has been proposed (*12*, *13*).

In this paper, we present the structure of the R2F protein of the enterobacterium *C. ammoniagenes* in the reduced and oxidized (met) state. From earlier structural studies of the *Salmonella typhimurium* R2F, modeling based on this structure, and sequence alignments, it was believed that the *C. ammoniagenes* R2F structure should be similar to *S. typhimurium* R2F (*14*). For this reason, the *S. typhimurium* R2F structure was used as the search model for molecular replacement to get initial phases for the data. Although similar, these two class Ib structures show differences in the overall structure and the geometry around the metal sites. The two R2Fs show differences compared to *E. coli* R2, the most striking being the lack of a $\beta$-sheet motif, making their general appearance more similar to the mouse R2. The hydrogen bonding pattern around the tyrosyl radical site is also different.

Another group of metal-carboxylate proteins are the manganese-dependent enzymes, e.g., arginase (*15*) and the di-manganese catalase (*16*, *17*). The metal binding motifs of these enzymes are similar to the di-iron carboxylate proteins. The apo (without metal) R2(F) proteins are capable of binding manganese to their iron binding sites (*18*), and we also present the structure of the manganese-substituted R2F from *C. ammoniagenes*.

It has been found that cell division and DNA synthesis in *C. ammoniagenes* are dependent on manganese (*19*), and it has been speculated that this dependence is correlated to ribonucleotide reductase (*20*, *21*). The *C. ammoniagenes* R2F has for this reason previously been assigned to a new class (IV) of ribonucleotide reductases (*22*). The manganese-substituted metal site is, however, not able to pass through the oxygen-activated redox cycle (*23*), and thus cannot form an active cofactor for the enzymatic reaction, which is additionally confirmed by the structure of the manganese-substituted form of *C. ammoniagenes* R2F. Although inactive, the manganese-containing center can give further spectroscopic information about the magnetic environment around the metal site.

## EXPERIMENTAL PROCEDURES

*Strains, Plasmids, and Materials.* The pIG056 plasmid coding for the gene *nrdF* from *C. ammoniagenes* under control of the T7 promotor was used for overproduction in the *E. coli* strain JM109(DE3), carrying the Lac promoter/T7 polymerase gene (Promega). Chemicals used were $MnCl_2$ (Merck), streptomycin sulfate (Sigma), ammonium sulfate (Merck), sodium ascorbate (KEBO), and Mohrs salt, $(NH_4)_2Fe(SO_4)_2$ (Merck).

*Overproduction and Purification of R2F from C. ammoniagenes.* The overproduction of R2F was conducted in rich media (LB). Cells were disrupted by X-press (Biox AB), the DNA was precipitated with 1.5% streptomycin sulfate, and the protein was precipitated with 60% ammonium sulfate as previously described (*23*). This resulted in an iron content of 0.5 Fe/R2F monomer (denoted apoR2F).

To reconstitute the iron center, 15 $\mu$L of $N_2$-saturated 50 mM Tris, pH 7.6, with 100 mM $(NH_4)_2Fe(SO_4)_2$ and 200 mM sodium ascorbate was added to 0.5 mL of 0.85 mM R2F, and incubated for 5 min at 25 °C and then cooled to 0 °C. The reconstitution mixture was desalted on a G25 (NAP-25) column using 50 mM Tris, pH 7.6. This resulted in the iron-containing protein (denoted R2F-Fe).

The R2F containing manganese (R2F-Mn) was grown with 2 mM $MnCl_2$ added to the medium. After X-press, DNA was precipitated with 1.5% streptomycin sulfate. The manganese content was 1.6 Mn/R2F monomer, and the iron content was 0.5 Fe/R2F monomer (*23*) (denoted R2F-Mn).

The different R2F samples were purified on a MonoQ (10/10) ionic exchange column as desribed (*23*) and concentrated by centrifugation in a Centricon 10 (Amicon) to a concentration of 0.6−1.1 mM before metal analysis.

*Iron and Radical Content Determination by UV−Vis.* The iron content before crystallization was detemined by a colorimetric method based on phenanthroline chelation of iron (*10*, *24*); 1.65 irons per monomer were obtained in the reconstituted sample. Radical content was determined by dropline analysis at 407 nm of the UV−vis spectrum on a Perkin-Elmer $\lambda 2$ spectrophotometer between 402 and 420 nm, $\epsilon_{407} = 3400\ M^{-1}\ cm^{-1}$ (*23*). The radical content was 0.26 rad/R2F monomer.

*Crystallization and Crystal Soaking.* The protein was crystallized using the hanging-drop method. Protein solution containing 10 mg/mL protein in 50 mM Tris-HCl at pH 7.5 was mixed in ratios varying between 1:1 and 3:1 (protein:reservoir) with the reservoir solution consisting of 30% w/v PEG 4k, 100 mM sodium citrate, and 200 mM ammonium acetate at pH 6−6.5. Crystals grew after about 20 days; one rhombohedral-shaped crystal form and one platelike crystal form grew under identical conditions. To obtain only the rhombohedral crystals (about $0.2 \times 0.2 \times 0.1$ mm) suitable for data collection, the drops were streak-seeded after a few days of equilibration.

Crystals of the apo protein as well as the iron-containing and manganese-substituted protein were grown. When later analyzing the electron density, it was obvious that the metal sites in the crystals from the Mn-containing protein were far from fully occupied. This is most likely because the citrate used in the mother liquor is a metal chelator and was able over time to remove the metal ions from the protein. This was not observed in the Fe-containing protein, probably because in this case the metals were present in the form of the oxo-bridged di-Fe(III) center which would be expected to be more tightly bound to the protein than the divalent metal ions.

To obtain the structure of the fully occupied Mn-containing site, crystals of the Mn-containing protein were first soaked in mother liquor containing 100 mM MES buffer instead of

Table 1: Data Statistics for the *C. ammoniagenes* R2F Structures

| data statistics R2F | oxidized Fe-containing | reduced Fe-containing | Mn-substituted |
|---|---|---|---|
| cell parameters (Å) | | | |
| *a* | 50.81 | 49.95 | 50.67 |
| *b* | 90.71 | 91.15 | 91.20 |
| *c* | 136.81 | 137.27 | 137.27 |
| space group | $P2_1$ | $P2_1$ | $P2_1$ |
| unique angle: $\beta$ (deg) | 91.24 | 91.27 | 91.45 |
| resolution (Å) | 30−1.85 | 25−2.25 | 25−2.0 |
| (outer shell) | (1.88−1.85) | (2.29−2.25) | (2.03−2.00) |
| no. of observations | 193418 | 135221 | 149319 |
| unique reflections | 101333 | 55206 | 77244 |
| $R_{merge}$[a] | 0.048 | 0.079 | 0.071 |
| (outer shell) | (0.260) | (0.294) | (0.209) |
| completeness (%) | 95.9 | 94.7 | 91.1 |
| (outer shell) | (94.7) | (96.4) | (85.4) |

[a] $R_{merge} = \Sigma_j\Sigma_h|\langle I_{hj} - I_h\rangle|/\Sigma_j\Sigma_h I_{jh}$ where $I_{hj}$ is the *j*th observation of reflection *h*.

Table 2: Refinement and Ramachandran Plot Statistics for the *C. ammoniagenes* R2F Structures

| refinement | oxidized Fe-containing | reduced Fe-containing | Mn-substituted |
|---|---|---|---|
| $R_{cryst}$[a] (%) | 15.8 | 16.3 | 17.7 |
| $R_{free}$[b] (5% of data) (%) | 21.3 | 23.8 | 23.6 |
| non-H atoms | 11219 | 10536 | 10667 |
| solvent molecules | 1528 | 849 | 980 |
| rms dev. bonds (Å) | 0.014 | 0.010 | 0.009 |
| rms dev. angles (deg) | 1.44 | 1.29 | 1.21 |

| Ramachandran plot (% of reidues) | oxidized Fe-containing | reduced Fe-containing | Mn-substituted |
|---|---|---|---|
| most favored | 97.2 | 96.4 | 97.0 |
| allowed | 2.8 | 3.6 | 3.0 |
| generously allowed | 0.0 | 0.0 | 0.0 |
| disallowed | 0.0 | 0.0 | 0.0 |

[a] $R_{cryst} = \Sigma||F_{obs} - F_{calc}||/|\Sigma_{obs}|$, where $F_{obs}$ and $F_{calc}$ are the observed and calculated structure factor amplitudes, respectively. [b] $R_{free}$ is equivalent to $R_{cryst}$ for a 5% subset of reflections not used in the refinement.

the citrate and then moved to the same solution containing 10 mM $MnCl_2$ and 15% glycerol for cryo protection for 30 min before being frozen. The reduced Fe site was obtained by soaking crystals of the apo protein in the same way except that the cryo solution contained 10 mM $Fe(NH_3)_2(SO_4)_2$, 1% dithionite, and 1 mM phenosafranin and the soak time was 1 h.

*X-ray Data Collection.* Crystals were cryo protected in reservoir solution supplemented with 15% glycerol or PEG 400, picked up in rayon loops (Hampton Research), and flash-frozen in liquid nitrogen.

Diffraction data were collected on a MAR 345 imaging plate or a CCD area detector (ADSC Q4 CCD) using synchrotron radiation (beam line I711 at the MAXII synchrotron in Lund, Sweden, or ID14-2 at ESRF Grenoble, France). Crystals were kept at 100 K during data collection using a cryosystem (Oxford Cryosystems); the data were processed and scaled using Denzo and Scalepack (*25*).

The crystals belonged to the monoclinic crystal system and could be assigned to spacegroup $P2_1$ based on systematic absences. The cell parameters are approximately $a = 51$ Å, $b = 91$ Å, $c = 137$ Å and the unique angle $\beta = 91.3°$. The asymmetric unit contains two dimers and has a calculated solvent content of 35%. Data statistics are shown in Table 1.

*Phasing.* Molecular replacement searches using the CNS software (*26*), with the sequence of the *C. ammoniagenes* protein threaded on the structure of the *S. typhimurium* R2F backbone as template, were performed to determine initial phases for the data. In the initial round of rotation and translation searches, only one significant peak was found. From the cell parameters and the size of the protein (329 residues), we suspected that there were 2 dimers in the asymmetric unit. To get a better model and to be able to find the second solution, a simulated annealing procedure was performed on the structure from the first solution (i.e., with less than 50% of the unit cell content), and the resulting model was used in the subsequent molecular replacement searches. This approach proved successful, and, when keeping the first solution fixed, we were able to, with the improved model, pick out the second. It should be noted that in the final refined structure there are no obvious differences between the noncrystallographically related dimers.

*Model Building and Refinement.* Interpretation of maps and model building was done using the Swiss Pdb Viewer (*27*) (www.expasy.ch/spdbv) on an iMac.

Structures were refined using the CNS software (*26*), and automated water building was done using the ARP/wARP program package (*28*). A total of 15 cycles of solvent building were performed; water molecules were added in densities above 3.2$\sigma$ in $F_o-F_c$ maps and removed if below 1$\sigma$ in $2F_o-F_c$ maps. The free *R*-value was calculated from 5% of the data and monitored throughout the refinement (Table 2).

Figures were created using either the Swiss Pdb Viewer and POV-Ray, Molscript (*29*), and Raster3D (*30*) or Bobscript, Robert Esnouf's extended version of Molscript.

## RESULTS

Three structures of *C. ammoniagenes* R2 have been determined to high resolution, with good *R*-values and stereochemistry (Table 2). The structures solved are of the protein in its reduced and oxidized iron-containing states as well as its manganese-substituted state. The substitution for manganese was made primarily because this protein has been proposed to be Mn-dependent (*20*, *21*), because spectroscopic data exist (*23*), and because comparisons to the Mn-substituted *E. coli* R2 (*18*) can be made.

*Overall Structure.* The *C. ammoniagenes* R2F is an all-helical homodimeric protein with 12 helices packed in a manner similar to that seen in the other R2s solved to date (*14*, *31*−*33*) (Figure 1). The main helix bundle in these proteins consists of eight helices denoted αA−αH; all these are also present in the *C. ammoniagenes* R2. In the structure of the *E. coli* protein, four additional helices, denoted α1−α4, are present. In *C. ammoniagenes* R2F, the helices corresponding to α1, α2, and α4 are also present. α3, however, has no counterpart in the *C. ammoniagenes* protein, and instead, αG is somewhat longer and starts directly after αF. The N-terminus of the *C. ammoniagenes* protein forms an additional 2-turn helix, denoted α0, embracing the other subunit of the protein. This leads to a very pronounced arm exchange between the monomers, in contrast to the *E. coli* and mouse proteins in which the N-terminus folds back onto

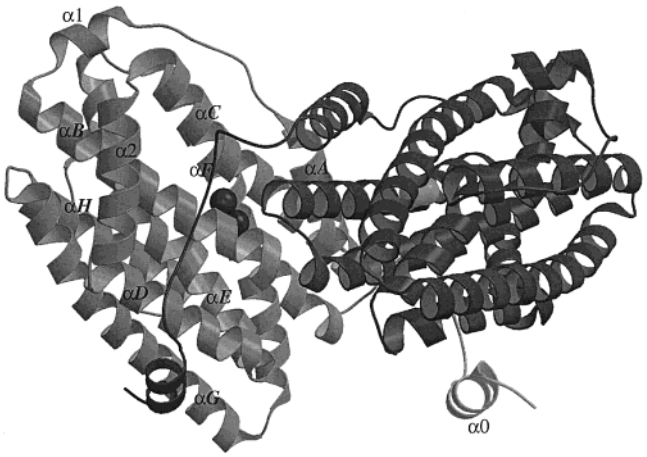


FIGURE 1: *C. ammoniagenes* R2 dimer. The different subunits are colored light and dark gray, respectively. The iron atoms in the dinuclear metal centers are shown as spheres. The nomenclature is adapted from ref (*31*). Note especially the N-terminal α0 helix leading to a very pronounced arm exchange between the monomers.

the same monomer. The *S. typhimurium* protein has a 10 residue shorter N-terminal sequence than the *C. ammoniagenes* protein and is thus lacking the residues forming the α0 helix. The pleated sheet part present in the *E. coli* protein is missing. From sequence alignments and the structures of the R2 proteins solved thus far, it seems that the prokaryote Ia proteins are the exceptions in this case.

*The Metal Site.* The metal binding site of *C. ammoniagenes* R2F consists of two histidines (H111 and H205) and four carboxylates (D77, E108, E168, and E202) as depicted in Figure 2.

The radical harboring tyrosine Y115 is situated further from the metal site than in the *E. coli* structure (about 7 Å in *C. ammoniagenes* compared to about 5 Å in *E. coli*); this gap is filled by a water molecule H-bonded to Y115 and D77. The longer distance and bridging water molecule is also seen in the structure of reduced *S. typhimurium* R2F and seems to be a general feature of the class Ib R2s.

In the reduced iron-containing metal site (Figure 2a), Fe1 and Fe2 are 4- and 5-coordinate, respectively. Fe1, which is closest to the radical harboring tyrosine Y115, has four monodentate ligands; H111, D77, E108, and E202. Fe2 has 1-coordination to H205, E108, and E202 while it is bidentally coordinated by E168. This situation is different from that in the reduced *E. coli* protein (*3*), in which both irons are 4-coordinate. No additional water ligands are seen in the *C. ammoniagenes* R2F reduced iron site apart from the water bridging between Y115 and D77. In the structure of the *S. typhimurium* protein, an additional water seems to be bridging the two iron ions (*14*). Compared to the E238 in the *E. coli* R2 site, which is almost totally symmetric, the E202 in *C. ammoniagenes* R2F is somewhat skewed in its coordination to the iron atoms.

The oxidized iron-containing metal site of *C. ammoniagenes* R2F shows large conformational changes of the ligands compared to the reduced site (Figure 2b). Fe1 is now 5-coordinate and Fe2 is 6-coordinate, and the irons are symmetrically bridged by a $\mu$-oxo bridge. Two additional water molecules are present in the site, and a fairly complex hydrogen-bonded network is created (Figure 3a). The water bridging between Y115 and D77 is still present in the

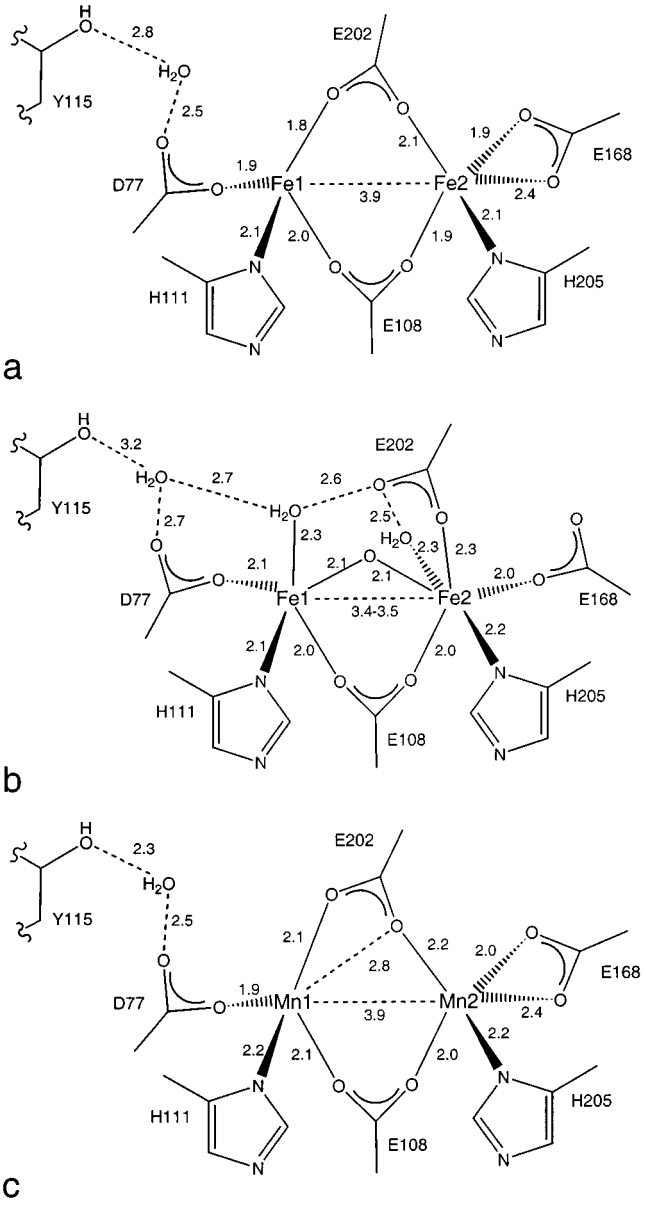


FIGURE 2: Schematic structure and coordination distances in angstroms of the metal centers in *C. ammoniagenes* R2. (a) Reduced Fe-containing site; (b) oxidized (met) Fe-containing site; (c) manganese-substituted site.

oxidized *C. ammoniagenes* R2F site, which seems not to be the case in the oxidized *S. typhimurium* R2F site.

It should be noted that the electron density of the oxidized Fe-containing crystals shows differences in the four non-crystallographically related metal sites. The most likely explanation for this is that they have suffered different degrees of X-ray reduction during exposure. Sites A and B show mixed conformations while site C seems almost entirely oxidized and site D mainly reduced. However, it cannot be totally ruled out that the oxidized site C has some contribution of a reduced site at low occupancy which would lead to a slight overestimation of the iron−iron distance. X-ray reduction has previously been noticed for the *S. typhimurium* class Ib R2 protein (*14*). It is also known to happen in the *E. coli* protein, but then only after thawing and refreezing of an exposed crystal (*3*).

The Mn-substituted site in *C. ammoniagenes* R2F is very similar to the reduced Fe-containing site but with slightly

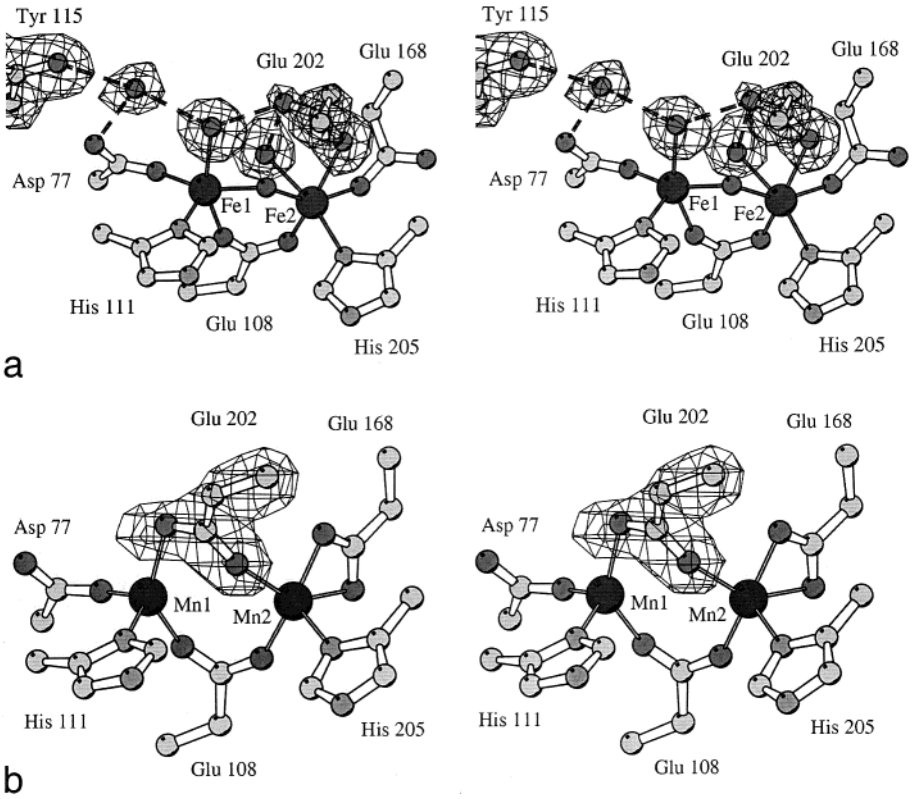


FIGURE 3: Stereoviews of (a) the oxidized (met) Fe-containing *C. ammoniagenes* site, omit maps of Y115, E202, and the water molecules contoured at 4.5$\sigma$; and (b) the manganese-substituted *C. ammoniagenes* site, omit map of E202 contoured at 4.5$\sigma$.

different coordination distances (Figure 2c). The E202 is even more skewed in its coordination to the metals with both oxygens fairly close to Mn1 (Figure 3b). This could explain the strong coupling between the two metal ions (*23*). No additional water is seen coordinating the Mn ions in this structure as seen in the Mn-substituted *E. coli* R2.

## DISCUSSION

The overall structure of *C. ammoniagenes* R2F is, as expected, most similar to the structure of *S. typhimurium* RNR R2 (*14*). This protein also belongs to the class Ib RNRs and has a sequence identity to *C. ammoniagenes* R2F of 66%. The structures can be superimposed with an rms deviation for the α carbons of 1.1 Å over the entire *S. typhimurium* R2F structure. There are no obvious differences which would lead to the suspicion of a different metal dependence for the *C. ammoniagenes* protein.

Compared to the *E. coli* and mouse R2s (*31*, *33*), the overall fold of *C. ammoniagenes* in the helical structure is surprisingly similar considering the low sequence identity (25 and 17% sequence identity, respectively). The iron-coordinating 4-helix bundles (118 residues) superimpose with an rms deviation of 1.2 (Figure 4a) and 1.3 Å (Figure 4b), respectively, for the α carbons. The same comparison of *C. ammoniagenes* R2F to *S. typhimurium* R2F gives an rms deviation of only 0.6 Å (Figure 4c).

The C-terminal part of the protein is disordered, as in the previously solved R2 structures. From an alignment of the thus far solved R2(F) structures (Figure 5), one can see that the disordering starts at essentially the same position in all the proteins (297 in *C. ammoniagenes*). This is a strong indication that this is really the biologically and functionally relevant position for the end of the ordered structure. In all bacterial R2(F) proteins, the structure ends with a short helix just before a conserved serine at which the structures seem to end. The mouse protein does not have this helix, and the disordering starts a few residues earlier in the sequence. A part of the *E. coli* R2 C-terminus has been solved in complex with the *E. coli* R1 protein (*34*); the ordered part of this peptide, which starts at a conserved glycine, is also indicated in the structural alignment. The structure of the last seven residues of the mouse R2 in complex with the mouse R1 protein has been determined by NMR methods. Interestingly, this does not seem to adopt the same conformation as the *E. coli* C-terminal peptide (*35*).

*Comparison of Class Ia and Ib.* Class I RNRs are divided into two classes according to sequence. Class Ia exists in eukaryotes, bacteria, viruses, and bacteriophages, while Ib has only been found in bacteria. In some species, the two subclasses coexist in the genome. There are also examples of species which harbor class I together with class II and/or class III. In both class Ia and class Ib, all the residues involved in the active site, radical transfer, and metal site (including the tyrosine that harbors the stable radical) are conserved. Both have the R1(E) dimer interface allosteric site which determines substrate specificity. In addition, the class Ia R1 proteins harbor an N-terminal overall activity site, which the class Ib R1 proteins are missing. During each reaction cycle, the R1(E) protein needs to be reduced. Class Ia uses either thioredoxin or glutaredoxin to transfer 2 reducing equiv from NADPH. Class Ib uses nrdH, a redoxin that is coded for on the class Ib operon, or glutaredoxin (*36*).

In the overall structure of the R2 subunits, however, there are no obvious features that are specific for the Ia and Ib

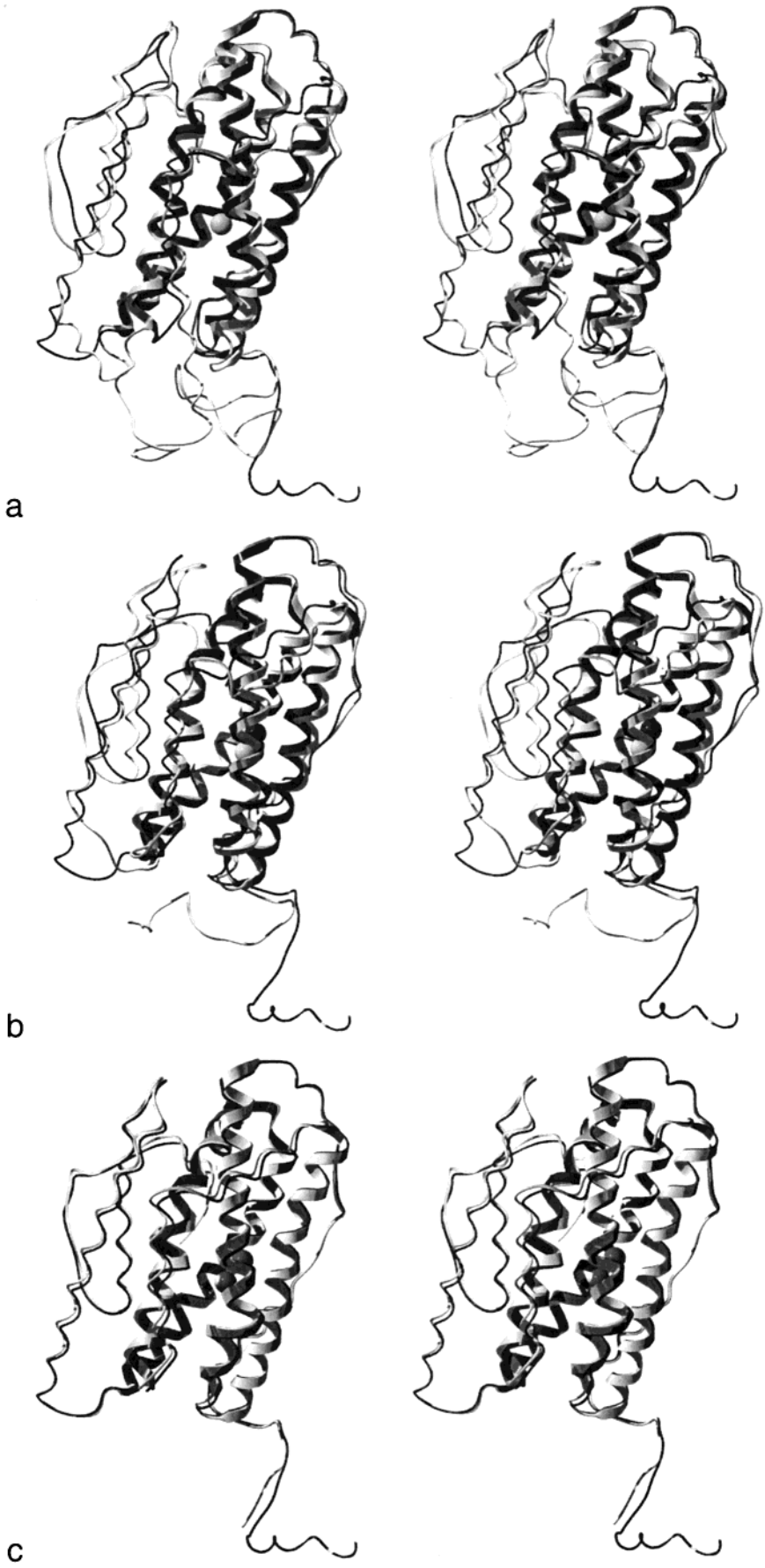


FIGURE 4: Stereoviews of superimposed R2(F) monomer structures. The iron-coordinating four-helix bundle is drawn as thicker helices. *C. ammoniagenes* is drawn in black and compared to (a) *E. coli* R2, (b) mouse R2, and (c) *S. typhimurium* R2F, all drawn in light gray.

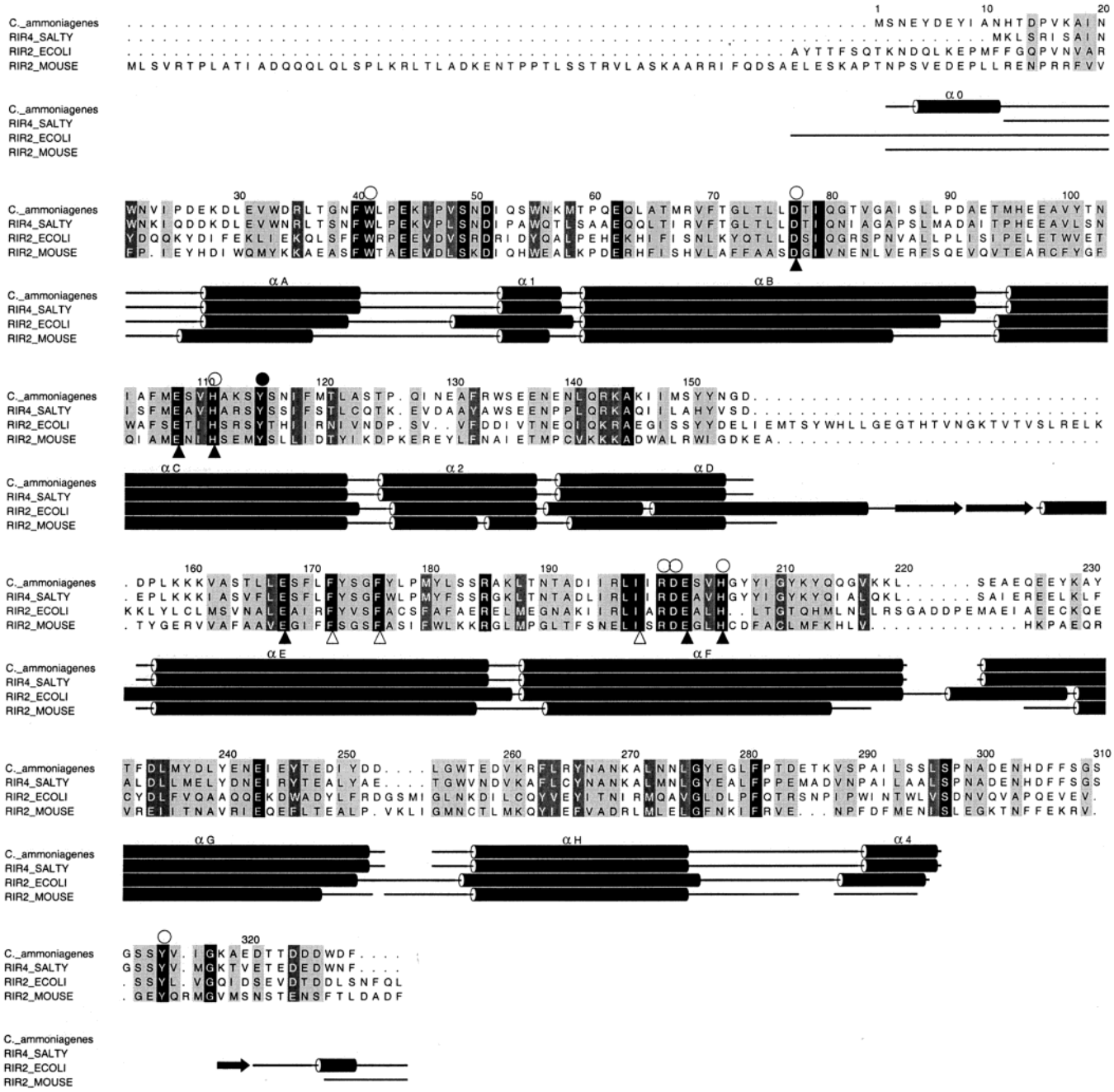


FIGURE 5: Structural alignment of the thus far solved R2(F) structures; the numbering and helix annotations correspond to *C. ammoniagenes*. Filled triangles (▲) represent metal ligands, open triangles (△) represent the hydrophobic pocket around the radical harboring tyrosine and Fe1, the filled circle (●) represents the radical harboring tyrosine, and open circles (○) correspond to the residues making up the hydrogen-bonded pathway proposed to be involved in radical transfer. The *C. ammoniagenes* sequence was taken from ref (*41*), and the others are the Swissprot entries RIR4_SALTY = *S. typhimurium* R2F, RIR2_ECOLI = *E. coli* R2, and RIR2_MOUSE = *M. musculus* (mouse) R2. The alignment was formatted using Alscript (*42*).

classes. The class Ib proteins share features with both class Ia proteins which are not shared between these. For example, the Ib proteins and the *E. coli* Ia protein share the C-terminal helix, absent from the mouse protein, while the Ib proteins and the mouse proteins all lack the $\beta$ motif present in *E. coli* R2 (Figure 5).

The metal sites, on the other hand, show differences distinguishing the Ia and Ib classes. The most obvious is the longer distance between the radical harboring tyrosine and the metal cofactor in the class Ib proteins; this distance is bridged by an additional water molecule in the reduced *S. typhimurium* protein. In the *C. ammoniagenes* protein, however, this water is present in all the structures solved. Recently a detailed mechanism at the structural level for oxygen activation and radical generation at these di-iron carboxylate sites has been proposed (*12*, *13*). In this mechanism, the proton/electron transfer from the tyrosine is made possible by a H-bonded path from the tyrosine to a terminal oxygen ligand in the H-abstracting intermediate X. Following this reasoning, the bridging water in the class Ib proteins would need to be present also in intermediate X. The presence of a water in this position, also in the more densely coordinated *C. ammoniagenes* oxidized site, supports the possibility for this water to be present also in intermediate

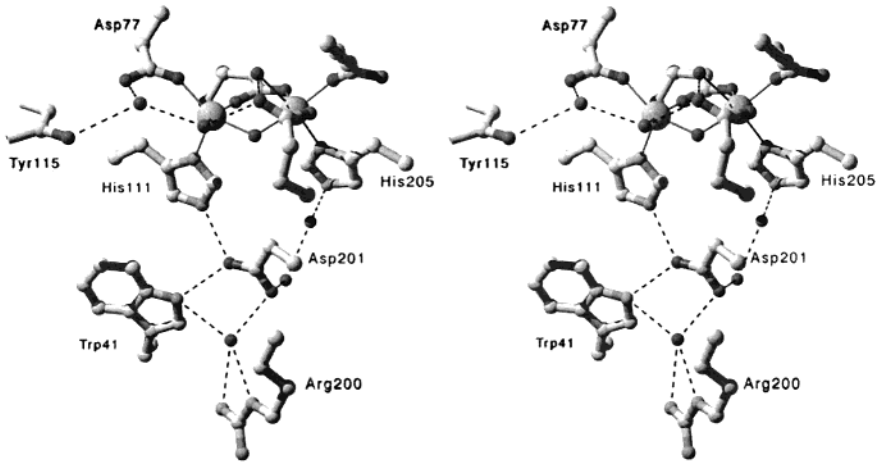


FIGURE 6: Hydrogen-bonded pathway from the oxidized iron site to the surface of the *C. ammoniagenes* R2 protein. The path from the H205 to D201 is made up of two water molecules which differ from the *E. coli* protein where Q43 takes this position. The corresponding residue in *C. ammoniagenes* (*36*) is a leucine.

X, which is presumed to be even more densely coordinated. The radical-containing site in *C. ammoniagenes* is likely to be similar to the oxidized site as presented in this work. When the radical is to be transferred to the R1 subunit to be used in ribonucleotide reduction, it is proposed to be done via a H-bonded pathway from the tyrosine to the active site in R1 [Figure 6 and ref (*37*)]. If proton transfer is essential also in this process, the novel water could mediate this transfer; alternatively, a direct tunneling of the electron from the tyrosine to, e.g., W41 (W48 in *E. coli*), not coupled to proton transfer, is in effect.

The hydrogen-bonded pathway seems to be conserved among all the R2(F) proteins except for changes in one position. *E. coli* R2 has a glutamine (Q43) which substitutes for the water molecules between H205 and D201 in *C. ammoniagenes* R2 and creates the path between the corresponding residues in *E. coli* (H241 and D237). This is a feature which, like the presence of the pleated sheet part, seems to be shared among the prokaryote class Ia R2s.

The arginine residue (R200) is located at the surface of the protein and is conserved among the R2(F) proteins and could play an important role in the radical transfer to the R1 subunit. Mutational studies of this residue are initiated and may give information on both the initial electron transfer to the metal site during the oxygen activation reaction, to yield intermediate X, as well as the radical transfer to R1.

*Mn-Substituted R2(F).* In the Mn-substituted *E. coli* R2 protein, a water is seen coordinating Mn2 (*18*); the metal−metal distance is in this case 3.6−3.7 Å. This distance is the same as the iron−iron distance in reduced *S. typhimurium* R2F, which also has a water coordinated to the metal site. In contrast, the metal−metal distances in reduced iron-containing *E. coli* R2, reduced iron-containing *C. ammoniagenes* R2F, and also the Mn-substituted *C. ammoniagenes* R2F are all 3.9 Å, and none of these metal sites has a water coordinated. It thus seems that the metal−metal distance in the metal sites with a II−II oxidation state is more determined by the absence or presence of a water ligand than the actual element bound. It could also be explained by slight differences in the conformation of one of the bridging carboxylates.

Comparing the manganese-substituted R2F structure presented here with the structure of manganese containing R2 from *E. coli* (*18*) shows that one bridging carboxylate has a slightly different conformation. The difference in magnetic coupling between the two manganese atoms in R2F from *C. ammoniagenes*, compared to R2 from *E. coli* (*18*, *38*), could be explained by the different conformation of the bridging carboxylate oxygen (Figure 2c), providing a single atom bridge instead of a O−C−O bridge in *E. coli* R2.

*C. ammoniagenes and Manganese. C. ammoniagenes* needs manganese for growth. Manganese-starved cells were found to have high concentrations of IMP (inositol monophosphate) and PRPP (5-phospho-α-D-ribosyl-1-pyrophosphate). More severely, they suffer from repressed DNA synthesis (*19*) but can perform transcription and translation. It was therefore suggested that the defects relate to the activity of the R2 subunit of ribonucleotide reductase (*20*, *21*) and that this protein was manganese-dependent. For other R2 proteins, where this has been investigated, however, iron and not manganese has been shown to constitute the radical generating cofactor (*18*). Recently, biochemical studies of the *C. ammoniagenes* R2 provide evidence against a manganese dependence. *Even* though manganese is taken up (2 ions/metal site), it cannot generate the radical that is required in the enzymatic reaction (*23*).

The two crystal structures with the reduced and oxidized iron center presented here are additional evidence that iron is redox-active in the protein and is thus likely to be able to form the radical site in R2F from *C. ammoniagenes*. The manganese-substituted protein, also exposed to oxygen, has a metal site coordination very similar to the Mn-substituted *E. coli* protein which is in its divalent (II−II) oxidation state (*18*). All three structures also show that two metal ions are taken up per metal site. Together, these results exclude a mononuclear manganese site as previously suggested (*39*). It also provides support against the notion that the dinuclear manganese site is oxidized by molecular oxygen (*20*, *21*) and supports an iron cofactor in the enzymatically active protein, as previously proposed (*23*).

Alternative explanations to the manganese requirement for growth could be related to the fact that class I ribonucleotide reductases need magnesium to form the holoenzyme complex [R1(E)−R2(F)]complex (*37*). Manganese may play this role in the *C. ammoniagenes* enzyme. Another explanation could relate to the known magnesium dependence of DNA

polymerases, which can be substituted by manganese (*40*). Transcriptional regulation through manganese-dependent DNA binding proteins is a further possibility.

Taken together, the previously published spectroscopical biochemical data and the present structural data strongly suggest that the manganese dependence of *C. ammoniagenes* must be looked for elsewhere.

## ACKNOWLEDGMENT

We thank Dr. Yngve Cerenius for assistance at the I711 beam line at MAX-lab in Lund and Dr. Ed Mitchell for assistance at the ID14-2 beam line at the ESRF in Grenoble.

## REFERENCES

1. Reichard, P. (1993) *Science 260*, 1773−1777.
2. Nordlund, P., and Eklund, H. (1995) *Curr. Opin. Struct. Biol. 5*, 758−766.
3. Logan, D. T., Su, X. D., Åberg, A., Regnström, K., Hajdu, J., Eklund, H., and Nordlund, P. (1996) *Structure 4*, 1053−1064.
4. Moenne-Loccoz, P., Baldwin, J., Ley, B. A., Loehr, T. M., and Bollinger, J. M., Jr. (1998) *Biochemistry 37*, 14659−14663.
5. Bollinger, J. M. J., Krebs, C., Vicol, A., Chen, S., Ley, B. A., Edmondson, D. E., and Huynh, B. H. (1998) *J. Am. Chem. Soc. 120*, 1094−1095.
6. Ling, J., Sahlin, M., Sjöberg, B. M., Loehr, T. M., and Sanders-Loehr, J. (1994) *J. Biol. Chem. 269*, 5595−5601.
7. Riggs-Gelasco, P. J., Shu, L. J., Chen, S. X., Burdi, D., Huynh, B. H., Que, L., and Stubbe, J. (1998) *J. Am. Chem. Soc. 120*, 849−860.
8. Willems, J. P., Lee, H. I., Burdi, D., Doan, P. E., Stubbe, J., and Hoffman, B. M. (1997) *J. Am. Chem. Soc. 119*, 9816−9824.
9. Shu, L., Nesheim, J. C., Kauffmann, K., Münck, E., Lipscomb, J. D., and Que, L. (1997) *Science 24*, 515−518.
10. Atkin, C. L., Thelander, L., Reichard, P., and Lang, G. (1973) *J. Biol. Chem. 248*, 7464−7472.
11. Silva, K. E., Elgren, T. E., Que, L., and Stankovich, M. T. (1995) *Biochemistry 34*, 14093−14103.
12. Andersson, M. E., Högbom, M., RinaldoMatthis, A., Andersson, K. K., Sjoberg, B. M., and Nordlund, P. (1999) *J. Am. Chem. Soc. 121*, 2346−2352.
13. Högbom, M., Andersson, M. E., and Nordlund, P. (2001) *J. Biol. Inorg. Chem. 6*, 315−323.
14. Eriksson, M., Jordan, A., and Eklund, H. (1998) *Biochemistry 37*, 13359−13369.
15. Kanyo, Z. F., Scolnick, L. R., Ash, D. E., and Christianson, D. W. (1996) *Nature 383*, 554−557.
16. Barynin, V. V., Hempsted, P. D., Vagin, A. A., Antonyuk, S. V., Melik-Adamyn, W. R., Lamzin, V. S., Harrison, P. M., and Artymiuk, P. J. (1997) *J. Inorg. Biochem. 67*, 196.
17. Waldo, G. S., and Penner-Hahn, J. E. (1995) *Biochemistry 34*, 1507−1512.
18. Atta, M., Nordlund, P., Åberg, A., Eklund, H., and Fontecave, M. (1992) *J. Biol. Chem. 267*, 20682−20688.
19. Oka, T., Udagawa, K., and Kinoshita, S. (1968) *J. Bacteriol. 96*, 1760−1767.
20. Schimpff-Weiland, G., Follmann, H., and Auling, G. (1981) *Biochem. Biophys. Res. Commun. 102*, 1276−1282.
21. Willing, A., Follmann, H., and Auling, G. (1988) *Eur. J. Biochem. 170*, 603−611.
22. Stubbe, J., and van der Donk, W. A. (1998) *Chem. Rev. 98*, 705−762.
23. Huque, Y., Fieschi, F., Torrents, E., Gibert, I., Eliasson, R., Reichard, P., Sahlin, M., and Sjöberg, B.-M. (2000) *J. Biol. Chem. 275*, 25365−25371.
24. Sahlin, M., Sjöberg, B. M., Backes, G., Loehr, T., and Sanders-Loehr, J. (1990) *Biochem. Biophys. Res. Commun. 167*, 813−818.
25. Otwinowski, Z. (1993) in *Proceedings of the CCP4 study weekend*, pp 56−62, SERC Daresbury Laboratory, Warrington, U.K.
26. Brünger, A. T., Adams, P. D., Clore, G. M., DeLano, W. L., Gros, P., Grosse-Kunstleve, R. W., Jiang, J.-S., Kuszewski, J., Nilges, M., Pannu, N. S., Read, R. J., Rice, L. M., Simonson, T., and Warren, G. L. (1998) *Acta Crystallogr., Sect. D 54*, 905−921.
27. Guex, N., and Peitsch, M. C. (1996) *Protein Data Bank Q. Newslett. 77*, 7.
28. Lamzin, V. S., and Wilson, K. S. (1993) *Acta Crystallogr., Sect. D 49*, 129−147.
29. Kraulis, P. J. (1991) *J. Appl. Crystallogr. 24*, 946−950.
30. Merritt, E. A., and Bacon, D. J. (1997) *Macromol. Cryst., Pt. B 277*, 505−524.
31. Nordlund, P., Sjöberg, B.-M., and Eklund, H. (1990) *Nature 345*, 593−598.
32. Nordlund, P., and Eklund, H. (1993) *J. Mol. Biol. 232*, 123−164.
33. Kauppi, B., Nielsen, B. A., Ramaswamy, S., Larsen, I. K., Thelander, M., Thelander, L., and Eklund, H. (1996) *J. Mol. Biol. 262*, 706−720.
34. Uhlin, U., and Eklund, H. (1994) *Nature 370*, 533−539.
35. Fisher, A., Laub, P. B., and Cooperman, B. S. (1995) *Nat. Struct. Biol. 2*, 951−955.
36. Jordan, A., and Reichard, P. (1998) *Annu. Rev. Biochem. 67*, 71−98.
37. Sjöberg, B. M. (1997) *Struct. Bonding 88*, 139−173.
38. Huque, Y., Røren Strand, K., Sahlin, M., Liu, A., Sjöberg, B.-M., Gräslund, A., Andersson, K. K., Atta, M., Fontecave, M., Barra, A.-L., Debaecker-Petit, N., Perret, E., Blasco, E., Latour, J.-M., and Le Pape, L. (2001), in preparation.
39. Griepenburg, U., Blasczyk, K., Kappl, R., Hüttermann, J., and Auling, G. (1998) *Biochemistry 37*, 7992−7996.
40. Pelletier, H., Sawaya, M. R., Wolfle, W., Wilson, S. H., and Kraut, J. (1996) *Biochemistry 35*, 12762−12777.
41. Fieschi, F., Torrents, E., Toulokhonova, L., Jordan, A., Hellman, U., Barbe, J., Gibert, I., Karlsson, M., and Sjöberg, B. M. (1998) *J. Biol. Chem. 273*, 4329−4337.
42. Barton, G. J. (1993) *Protein Eng. 6*, 37−40.

BI011429L